Spatial distribution of Ar on the Ar-ion-induced rippled surface of Si

Debi Prasad Datta and Tapas Kumar Chini*
Surface Physics Division, Saha Institute of Nuclear Physics, 1/AF Bidhannagar, Kolkata 700 064, India
(Received 23 November 2004; revised manuscript received 25 February 2005; published 9 June 2005)

We have measured spatial distribution of Ar atoms on the rippled surface generated on Si undergoing 60 keV Ar bombardment at a 60° angle of ion incidence. Elemental mapping and line scans using energy dispersive x-ray spectrometry attached in a scanning electron microscope confirmed that subsequent to the interpeak shadowing of incident ion flux, most of the argon atoms are incorporated around the middle part of the front slope of ripple facing the ion beam as compared to the rear slope. The spatial extension of the argon rich phase amounts about half of the ripple wavelength. The experimentally observed compositional heterogeneity between the two faces of the ripples agrees reasonably good to the well-known Monte Carlo ion simulator TRIM based theoretical calculations.

DOI: 10.1103/PhysRevB.71.235308 PACS number(s): 68.37.Hk, 68.35.Ct, 79.20.Rf, 81.16.Rf

I. INTRODUCTION

Development of periodic ripple morphology on solid surfaces undergoing erosion by obliquely incident ion bombardment has become a subject of intense research[1,2] in recent years because the controllable (micrometers to nanometers scale) wavelength and amplitude of such self-organized patterns makes them good candidates for possible application such as x-ray/optical grating or templates for growing low dimensional structure for nanotechnology.[3] The linear instability theory of ion bombarded surface, developed by Bradley and Harper (BH),[4] predicts formation of sinusoidal ripples where wavelength remains constant but amplitude grows exponentially with bombardment time. Our recent atomic force microscopy (AFM) study[5] of the ripple morphology for 60 keV $Ar \rightarrow Si$ at 60° angle of ion incidence shows that as the bombardment time increases, a critical value of the ratio of amplitude to wavelength is reached as predicted by Carter's geometrical argument[6] for which interpeak shadowing of incident ion flux distorts the sinusoidal ripple habit to faceted one. Neither BH theory[4] nor the more generalized theory developed by Cuerno and Barabasi (CB) (Ref. 7) and later by Makeev, Cuerno, and Barabasi (MCB) (Ref. 8) could explain such dynamical behavior of ripple pattern where shadowing phenomena is observed. The appearance of a ripple or a slope results immediately in local angles of ion incidence deviating from the overall one. Hence the local density of bombarding ions starts to deviate from the average one even much earlier than when the shadowing occurs. When the shadowing condition is reached the front slope of the ripples facing the ion beam will have more ions with an angle of incidence close to the local surface normal than the opposite face where the local angle of ion incidence is close to grazing causing most of the ions to be reflected instead of being implanted. Consequently, the penetration depth of ions that enter the front slopes is larger than of those that enter the back slopes. So a larger depth of the front slope will be affected both structurally and compositionally as compared with the rear slopes. Indeed, a structural variation with the formation of a thicker surface amorphous layer on the slope facing the ion beam has been observed in our recent cross-sectional transmission electron microscopy (XTEM) study[9] of (50–120 keV) Ar-ion (incident at 60°) induced Si surface ripples as depicted schematically in Fig. 1. However, the compositional variation over such medium kilo-electron-volt Ar-ion-induced Si surface ripples has not been addressed so far either theoretically or experimentally though such studies have been done at low (2–10 keV) energy for oxygen-ion-induced ripple formation on silicon by Homma *et al.*[10]

For ripple generation using low kilo-electron-volt ion beams with low angle of ion incidence, interpeak shadowing of the incident ion flux is not observed in general because the amplitude is much smaller than the wavelength of the ripples. As a result, influence of surface composition change caused by local incorporation of implanting ions on ripple evolution has been ignored in many cases even though possibilities of the existence of spatial inhomogeneities in ion-bombardment induced ripples was predicted[11] earlier. However, recent simulation[12] shows that for technological application, such as to fabricate nanowires, one should use high kilo-electron-volt obliquely incident ion beam that gives rise to V-shaped ripple pattern. For such a high energy induced corrugated pattern with high amplitude, the simulation

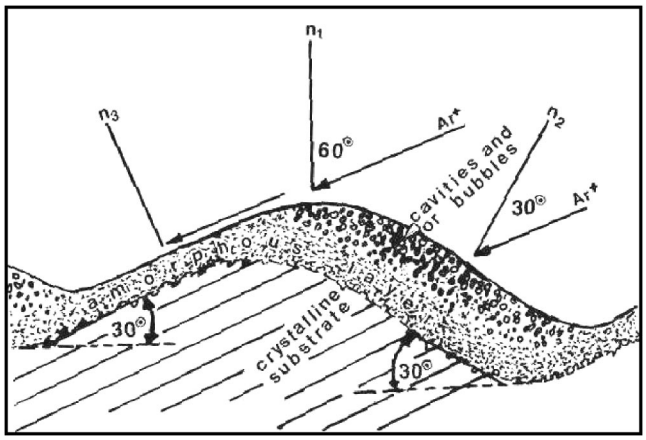

FIG. 1. Schematic diagram showing the structure and morphology of a ripple feature obtained from TEM measurements (see Ref. 9 for details).

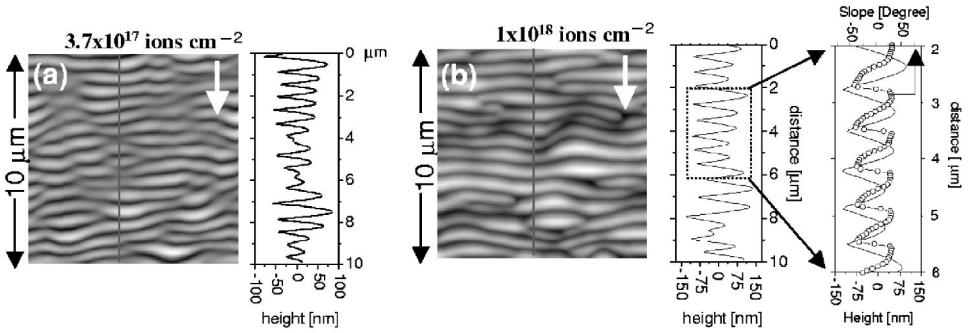

FIG. 2. Representative AFM images of the Ar bombarded Si surfaces with a fixed ion flux of 18 μA cm^{-2} for ion fluence 3.7×10^{17} ions cm^{-2} (a) and 1×10^{18} ions cm^{-2} (b). The height profiles shown with each of the images are taken along the solid line drawn over the images. Arrow mark shows the direction of the projection of ion flux on to the surface. The portion of the height profile of (b) selected by the dotted box is also shown along with the calculated slope angle variation (open circles) over the height profile. The lower half shows the amplitude, wavelength and their ratio for three different fluences.

Table 1

	3.7x10^{17} ions cm^{-2}	1x10^{18} ions cm^{-2}	1.5x10^{18} ions cm^{-2}
Amplitude (w) [nm]	56 ±2	110 ±3	132 ±15
Wavelength (l) [nm]	670 ±14	752 ±15	790 ±35
w : l ratio	0.08	0.14	0.16

has not considered the unavoidable effect of shadowing and the associated nonuniform incorporation of implanting ions that may cause distortion of the desired profile. The purpose of the present paper is to investigate the lateral distribution of argon atoms over the silicon surface undergoing erosion by 60 keV argon bombardment at a 60° angle of ion incidence in the sputtering time range which includes formation of a ripple pattern before and after shadowing transition. We attempt to explore how the compositional heterogeneity develops on the ripple slopes using the energy dispersive x-ray spectrometry (EDS) technique apart from using atomic force microscopy (AFM) for morphological analysis.

II. EXPERIMENT

The ion bombardment of the mirror polished surface of small pieces of Si samples [cut from a *p*-type B doped Si(001) single crystal wafer] was performed in a high current ion implanter.[13] The samples were bombarded with 60 keV Ar^+ beam at a 60° angle of ion incidence (with respect to surface normal of the samples). The ion flux was maintained at around 18 μA cm^{-2} and the ion fluence varied from 3.7×10^{17} ions cm^{-2} to 1.5×10^{18} ions cm^{-2}. After irradiation, the samples were investigated by atomic force microscopy (AFM) in contact mode under ambient condition for quantitative morphological analysis.

In order to evaluate the spatial distribution of Ar atoms for the same samples that were used for AFM analysis the x-ray elemental mapping was performed using the EDAX energy dispersive x-ray spectrometer (EDS) attached with the FEI QUANTA 200F Schottky field emission gun scanning electron microscope (FEG SEM) with the electron acceleration at 6 KV that sets a probe diameter of about 4 nm. Such low electron acceleration voltage brings the depth of x-ray generation more toward the surface of the probed sample making the bulk/thin film analyzing EDS technique surface sensitive. Consequently, the implanted Ar atoms confined within a few hundred nanometers from the surface of the present Ar bombarded Si samples can be detected efficiently. Care was also taken to orient the samples within the analyzing chamber of the scanning electron microscope (SEM) properly with respect to the peaks and valleys of ripple morphology so that x-ray emitted at a point is not absorbed by the adjacent high amplitude peak and maximum signal is collected by the detector. As a result, ripples generated up to those ion fluence were selected for which the maximum amplitude of the ripple was not a hindrance for x-ray analysis. The 256×200-pixel x-ray maps were obtained using a dwell time of 400 ms per pixel by selecting Si $K\alpha$ (1.74 keV) and Ar $K\alpha$ (2.95 keV) as the characteristic x-ray peaks. Associated with the computer based multichannel analyzer (MCA), the images were obtained in three different frames: the secondary electron image; the x-ray micrograph of the silicon substrate; and the X-ray micrograph of argon.

III. RESULTS

In Figs. 2(a) and 2(b) we report two representative AFM images showing the ripple morphology developed on 60 keV Ar bombarded Si surfaces at a 60° angle of ion incidence. Also shown are the height profiles taken along the line drawn on the images. That the orientation of the observed ripples is perpendicular to the projection of ion beam flux on to the surface as indicated by the arrow marks on each AFM images is consistent with the BH theory.[4] Following the method employed in our recent work[5] to determine the ripple wavelength and amplitude quantitatively, we evaluate the height difference correlation function[14] $G^{1/2}(r)$ of the AFM data, with $G(r)=\langle(h_i-h_j)^2\rangle$, where h_i and h_j are the heights of the surface at two locations separated by a distance r, and the brackets signify an average over pairs of points i and j. The ripple amplitude (W) and wavelength (l) thus determined from the AFM image analysis are tabulated in Fig. 2. For a

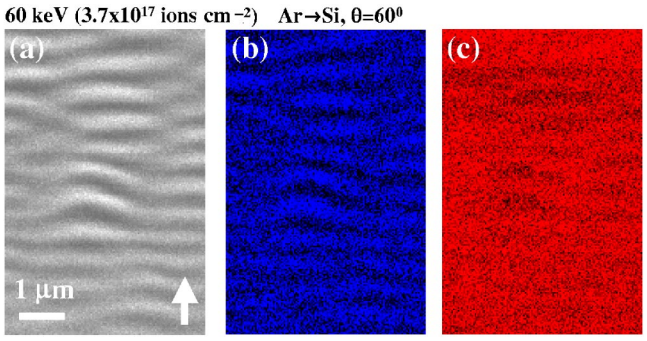

FIG. 3. (Color online) Showing SEM image (a), x-ray map of Ar (b) and Si (c) over the Si surface ripples for the Ar fluence of 3.7×10^{17} ions cm^{-2}.

sinusoidal ripple with the height profile approximated by $h = W\sin(2\pi x/l)$ Carter[6] has shown that the limiting condition to avoid interpeak shadowing of the incident ion flux is $\tan(\pi/2-\theta)\geqslant 2\pi W/l$ which places an upper limit on W/l for any ion incidence angle θ (with respect to the surface normal of the initial macroscopic flat surface). For the present experimental situation θ being 60°, the maximum tilt angle of the slope of the ripples should be thus $\left(\frac{\pi}{2}-\frac{\pi}{3}\right)=30°$ or $W/l\leqslant 0.09$ to avoid shadowing.

The EDS x-ray maps along with SEM secondary electron images of ripples generated on Si at different Ar doses are depicted in Figs. 3–5. Bright areas in the SEM images are ripples' crests whereas the bright areas in the x-ray elemental maps denote higher concentration of the respective element. For the case of Si surface undergoing Ar bombardment at 3.7×10^{17} ions cm^{-2}, regions of large roughness with a longer wavelength coexists with the regions of small roughness as it appears from the AFM image of Fig. 2(a) and SEM image of Fig. 3(a). Obviously the slopes developed by the regions of large roughness causes substantial variations in the local angle of ion incidence compared to the slopes developed by the features with small amplitude or roughness. As a result, spatially separated Ar rich phases start to appear in the regions of large roughness as verified from the x-ray Ar map of Fig. 3(b) analyzed over the area shown in the SEM images of Fig. 3(a). With increased ion fluence or bombardment time the large-roughness regions cover the whole surface and one notices the pronounced shadowing effect as observed from the W/l ratio of Fig. 2 beyond the dose 3.7×10^{17} ions cm^{-2}. As a result, the x-ray Ar maps of Figs. 4(b) and Fig. 5(b) corresponding to the SEM images of Figs. 4(a) and 5(a), obtained from the rippled surfaces produced at 10^{18} ions cm^{-2} and 1.5×10^{18} ions cm^{-2} show significant development in the spatial separation of Ar rich phases over a large area of sputtered region.

We also carried out EDS line scan measurements of Si Kα and Ar Kα signals along the line shown on the SEM images of Figs. 4(a) and 5(a) in the same region from where elemental mapping were taken. The straight lines joining each pair of number $(1\rightarrow1',2\rightarrow2',3\rightarrow3')$, the unprimed number representing the maxima of Ar intensity and the primed number denoting its corresponding location on the line of EDS scan on the SEM image, can be used as markers to compare the position of the maxima of Ar intensity with respect to the

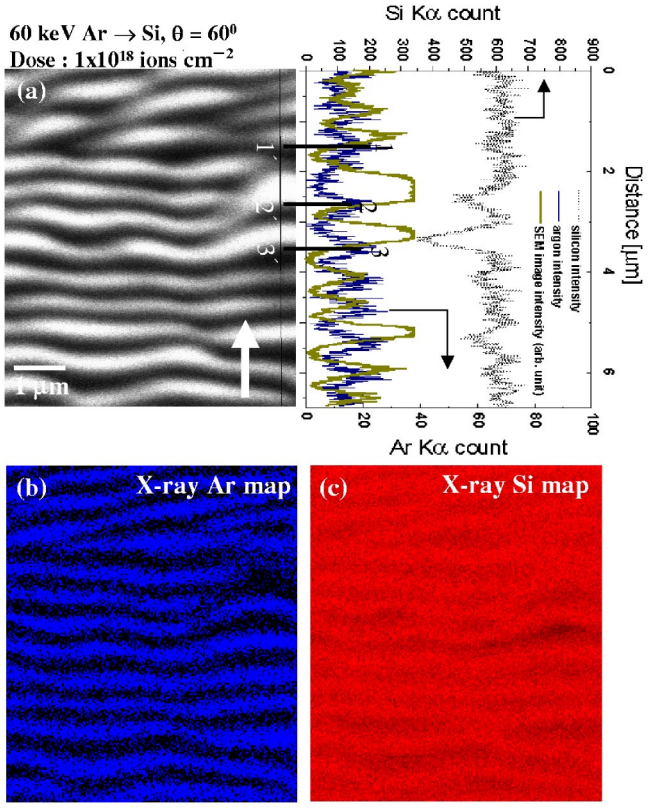

FIG. 4. (Color online) Showing SEM image (a) along with the SEM image intensity profile, Ar and Si intensity profile obtained from EDS line scan taken along the line shown on the SEM image for the Ar fluence of 1×10^{18} ions cm^{-2}. Arrow mark on the SEM image indicates the direction of the projection of ion flux on to the surface. Also shown are the x-ray maps of Ar (b) and Si (c).

slope of ripples. The middle points of the alternate bright and dark bands of the SEM images represent the peaks and valleys of the ripple morphology. It is seen that the markers, associated with the maxima of Ar intensity do not lie on the middle of the bright regions but lie toward the side of the darker bands of the SEM image. Comparison of the SEM image intensity profile and the Ar intensity profile reveals that maxima of Ar intensity is not located at the peaks of ripples but more towards the middle part of the front slope (facing the ion beam) of the ripples generated under shadowing condition. Assuming the oscillatory signals of the EDS line scans of Ar as Gaussian shaped, the full width at half maximum (FWHM) of such Gaussian distribution can be taken as a measure of the spatial extension of Ar distribution along the wave vector (shown by arrow mark on the SEM or AFM images of Figs. 2–5) of the ripple pattern. For the ripples generated at the dose 1×10^{18} ions cm^{-2} the average FWHM is 300 nm and the average FWHM is 400 nm at 1.5×10^{18} ions cm^{-2}. The spatial extension of the Ar rich phase occupies about 40% and 50% of the wavelength of the ripples produced at the corresponding doses. Also we found, the relative Ar concentration varies from about 1 at. % to 4 at. % as one probes from bottom to top along the front slope of ripples implying that upward part of the front slopes are Ar rich and valleys are Ar deficient. This variation of the concentration level along the front slope is found to remain

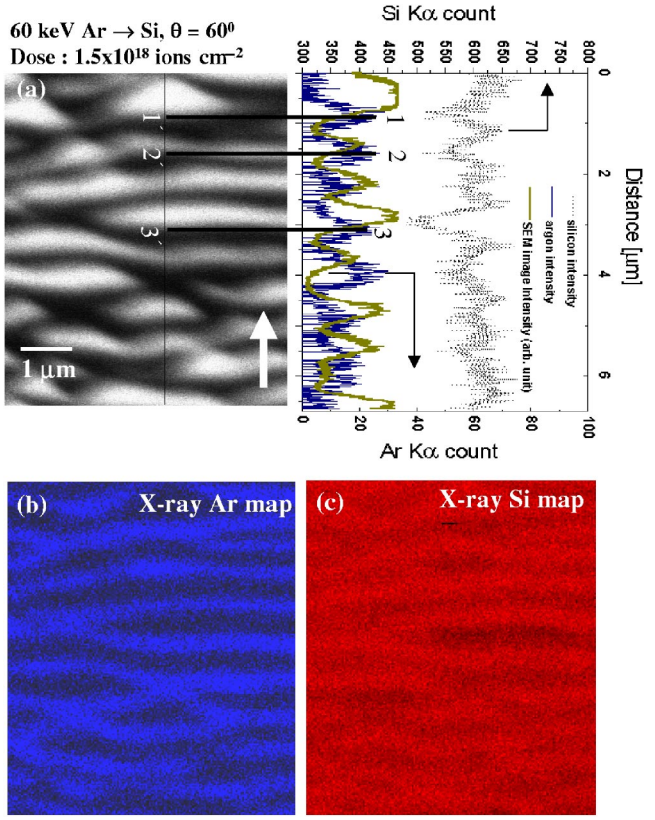

FIG. 5. (Color online) Showing SEM image (a) along with the SEM image intensity profile, Ar and Si intensity profile obtained from EDS line scan taken along the line shown on the SEM image for the Ar fluence of 1.5×10^{18} ions cm^{-2}. Arrow mark on the SEM image indicates the direction of the projection of ion flux on to the surface. Also shown are the x-ray maps of Ar (b) and Si (c).

more or less constant for rippled surface generated in the ion fluence ranging from 10^{18} ions cm^{-2} to 1.5×10^{18} ions cm^{-2} implying that a steady state or saturation condition is reached when the concentration of implanted atoms remains constant even with further bombardment. Although, the roughness of the bombarded surface may introduce a slight inaccuracy in the quantification of Ar level but they are correct to the order of magnitude as verified by Rutherford backscattering spectrometry (RBS) (not shown here). Regarding the variations of the Si intensity over the sputtered surfaces, the EDS line scans show some dips of the Si intensity at the positions of the maxima of Ar intensity, the effect being prominent at higher dose (namely at 1.5×10^{18} ions cm^{-2}).

IV. DISCUSSION

In our earlier XTEM measurements[9] of the cross section of ripple morphology as depicted schematically in Fig. 1, we observed the formation of cavities/bubbles at the subsurface region of the front slopes of ripples facing the ion beam direction whereas no such bubbles were detected at the rear slopes of the ripples. As the compositional analysis of the present study shows the maximum of the Ar intensity lies on the front slopes, it can now be said that the maximum amount of implanted Ar atoms giving the Ar signal in the

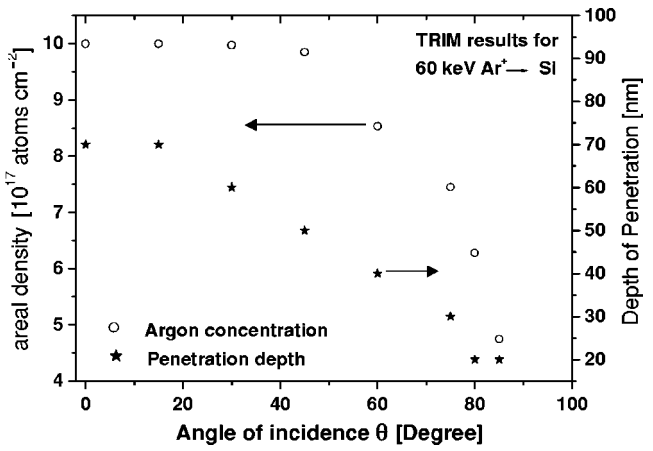

FIG. 6. Plots showing the variation of areal density and penetration depth of Ar as a function of angle of incidence as calculated from TRIM simulation for 60 keV Ar bombardment on Si.

EDS mapping or line scans are presumably trapped within the bubbles. Also the dips of the Si intensity at the maxima of Ar intensity may be indicative of the reduction of the Si concentration at the subsurface of the bombarded ripple slopes which is also consistent with the light contrast of the TEM images of the ripples as observed in Ref. 9. However, a crucial question is why the maxima of Ar content lie at midway of the front slopes? To answer this question we try to give a theoretical estimation based on the calculation using the well-known Monte Carlo ion simulator code TRIM (Ref. 15) as follows and then to compare it with our experimental observation.

We calculate the variation of Ar ion penetration depth in Si as a function of angle of ion incidence. Then we estimate the total number of implanted Ar atoms from the area of the implantation profile underneath the Si surface for each ion incident angle. The argon concentration measured by EDS is in atomic fraction while the same estimated by TRIM in the present case is in areal density (atoms/cm^2). We will use in our subsequent discussion areal density instead of concentration because concentration can mean both areal density and atomic fraction. As it is difficult to know the density of the Si matrix in the presence of bubbles/cavities in the amorphous phase of subsurface region under the present bombardment condition we take the default values (provided by the TRIM program) of density as well as other parameters like surface binding energy and bulk binding energy of the crystalline Si to get an approximate theoretical picture. According to TRIM, the typical sputter yield Y for 60 keV $Ar\rightarrow Si$ is 1.92 atoms/ion at $\theta=0°$ (normal ion incidence) and 2.62 atoms/ion at $\theta=30°$ (typical local ion incident angle on the front slopes of ripples formed in the shadowing regime). In Fig. 6 we show the variation of the areal density of Ar and Ar ion penetration depth in Si as a function of incident angle. From Fig. 6, it is observed that Ar concentration is maximum for higher penetration depths and remains constant corresponding to the angle of ion incidence up to about 45° and falls sharply with the incident angle between 70° and 90°. We will see that the angle of ion incidence along the slope of ripples does not remain constant and we will project this

scenario on the slope of ripples to get an idea of the location of the maximal of Ar content. But before that let us understand the geometry of the ripple slopes. We consider the slope to be defined by the slope angle θ_s, which is 30° for the case of Fig. 1 based on our earlier XTEM measurement near the region of shadowing condition which is really applicable for the rippled surface generated in the present studies around the dose of 10^{18} ions cm^{-2}. If the initial ion incident angle be θ with respect to the flat surface normal (n_1), the local ion incidence angles with respect to local surface normals (n_2 or $n3$) on the front and rear slope will be thus $\theta_f = (\theta - \theta_s)$ and $\theta_r = (\theta + \theta_s)$, respectively. It is interesting to note that θ_s on the ripple slope does not remain constant and we calculate the slope angles from the height profiles of AFM image [Fig. 2(b)]. The slope calculation was performed from the portion of the height profiles surrounded by the dotted box. The plot of the selected height profiles (continuous line) along with the slope profile (open circles) is shown at the top right-hand corner of Fig. 2. On average, a maximum slope angle of ~32° (exceeding the critical condition of shadowing) persists approximately at the middle of the front slope of ripples. This means, on average, the local angle of ion incidence at the middle of the ripple's slope will be 60°–32° =28°, corresponding to the angular regime where the maximum of the Ar concentration in the theoretical plot of the concentration versus incidence angle plot (Fig. 6) occurs. This is consistent with the observation of the maximum Ar intensity on the midway of the front slope of ripples as depicted in the SEM image along with EDS line scans of Figs. 4(a) and 5(a). On the other hand, the slope angle near the valleys are roughly −25°, yielding local ion incidence angle near valleys being around 85° that corresponds to a minimum level of Ar concentration in the plot of Fig. 6 and may explain the reason why we see the minimum level of Ar in the valleys with respect to the SEM image versus EDS line scans of Figs. 4(a) and 5(a). Thus, if we project the theoretical scenario of the plots of Fig. 6 on the slope of ripples to get an idea of the spatial distribution of the Ar, reasonably good agreement is found between experiment and theory.

Another quantity which varies as a function of ion incidence angle is the sputtering yield (atoms removed per incident ion). Although it is very difficult to determine the sputtering yield experimentally in the presence of ripple morphology as in the present case, it is well-known for semiconductors which are amorphized easily by medium kiloelectron-volt heavy ion bombardment, maximum of sputtering yield occurs somewhere between 70° and 75° (Ref. 16) in the absence of rough morphology. It is mainly for this reason that the sputtering yields for the front slopes and back slopes are different. This difference will cause propagation of ripples. However, at present we do not know the extra effect related to various levels of Ar incorporation on ripple morphology, especially after long time bombardment. Interestingly, Chelgren *et al.*[17] has shown a direct relationship between the sputter yield Y and the surface fraction C_s of implanted species as $C_s \sim 1/(Y+1)$. This also implies a higher concentration of Ar in the slower eroding front slopes as observed in the present results.

V. CONCLUSION

In conclusion, using energy dispersive x-ray spectrometry (EDS) elemental mapping and line scans, we have measured spatial distribution of Ar atoms on the rippled surface generated on Si undergoing 60 keV Ar bombardment at a 60° angle of ion incidence. We show that interpeak shadowing of the incident ion flux beyond a fluence $\sim 3 \times 10^{17}$ ions cm^{-2} causes a preferential incorporation of incident Ar ions at subsurface of about midway of the front slopes of ripples facing the ion beam as compared to the rear slopes. The present authors have measured actual spatial inhomogeneities in ion-bombardment induced ripples, as predicted earlier.[11]

*Electronic address: tapask.chini@saha.ac.in

[1] U. Valbusa, C. Boragno, and F. B. de Mongeot, J. Phys.: Condens. Matter **14**, 8153 (2002).
[2] J. Erlebacher, M. J. Aziz, E. Chason, M. B. Sinclair, and J. A. Floro, Phys. Rev. Lett. **82**, 2330 (1999).
[3] S. Rusponi, G. Costantini, F. Buatier de Mongeot, C. Boragno, and U. Valbusa, Appl. Phys. Lett. **75**, 3318 (1999).
[4] R. M. Bradley and J. M. E. Harper, J. Vac. Sci. Technol. A **6**, 2390 (1988).
[5] D. P. Datta and T. K. Chini, Phys. Rev. B **69**, 235313 (2004).
[6] G. Carter, J. Appl. Phys. **85**, 455 (1999).
[7] R. Cuerno and A. L. Barabasi, Phys. Rev. Lett. **74**, 4746 (1995); R. Cuerno, H. A. Makse, S. Tomassone, S. T. Harrington, H. E. Stanley, *ibid.* **75**, 4464 (1995).
[8] M. A. Makeev and A. L. Barabasi, Appl. Phys. Lett. **71**, 2800 (1997); M. A. Makeev, R. Cuerno and A. L. Barabasi, Nucl. Instrum. Methods Phys. Res. B **197**, 185 (2002).
[9] T. K. Chini, F. Okuyama, M. Tanemura, and K. Nordlund, Phys. Rev. B **67**, 205403 (2003).
[10] Y. Homma, A. Takano, Y. Higashi, Appl. Surf. Sci. **203–204**, 35 (2003).
[11] S. Rusponi, G. Costantini, C. Boragno, and U. Valbusa, Phys. Rev. Lett. **81**, 4184 (1998).
[12] J. Kim and B. Kahng and A.-L. Barabasi, Appl. Phys. Lett. **19**, 3654 (2002).
[13] T. K. Chini, D. Datta, S. R. Bhattacharyya, and M. K. Sanyal, Appl. Surf. Sci. **182**, 313 (2001).
[14] J. Lapujoulade, Surf. Sci. Rep. **20**, 191 (1994).
[15] Available from the web site: www.srim.org
[16] T. K. Chini, S. R. Bhattacharyya, D. Basu, and J. P. Biersack, Radiat. Eff. Defects Solids **127**, 349 (1994).
[17] J. E. Chelgren, W. Katz, V. R. Deline, and C. A. Evans, Jr., J. Vac. Sci. Technol. **16**, 324 (1979).